

Imaging of flexural and torsional resonance modes of atomic force microscopy cantilevers using optical interferometry

Michael Reinstaedtler ^{a,*}, Ute Rabe ^a, Volker Scherer ^b,
Joseph A. Turner ^c, Walter Arnold ^a

^a *Fraunhofer Institute for Non-Destructive Testing, Bldg. 37, University, D-66123 Saarbrücken, Germany*

^b *Federal-Mogul Burscheid GmbH, Bürgermeister-Schmidt-Str. 17, D-51399 Burscheid, Germany*

^c *Department of Engineering Mechanics, University of Nebraska, Lincoln, NE 68588-0526, USA*

Abstract

Commercial rectangular atomic force microscope cantilever beams made of silicon were set into vibration, using a piezoelectric ultrasonic transducer coupled to the chip of a cantilever. The transducer was excited with continuous rf in the frequency range of 100 kHz to 3 MHz. The vibrations were monitored using an optical Michelson heterodyne-interferometer allowing the surface of the cantilever under examination to be scanned with a lateral resolution of several μm . A number of free torsional and flexural vibration modes of the beams were imaged quantitatively. Comparison of the experimental resonance frequencies and the amplitude and phase distribution of the modes to theoretical models showed that asymmetries in the beam strongly influence the vibrational behavior of the beam. The consequences for quantitative local stiffness measurements are discussed.

© 2003 Elsevier Science B.V. All rights reserved.

Keywords: Atomic force microscopy; Acoustic waves; Models of non-linear phenomena

1. Introduction

Since the invention of the atomic force microscope (AFM) [1] several different quasi-static and dynamic operating modes have been developed, for example friction force microscopy (FFM) [2] or atomic force acoustic microscopy [3]. During the past few years, many groups have been im-

proving the quasi-static FFM technique [4,5] to a dynamic method, expanding the possibility to examine the origin of friction on a nanoscale [6–18] without the shortcomings of conventional FFM, which are time-consuming measurements with high noise and unstable friction imaging.

One crucial component for all AFM-operating methods is the flexible force-sensing cantilever [19]. These micro-fabricated AFM cantilevers can be regarded as miniature elastic beams with characteristic bending and torsional vibration modes. By means of elasticity theory it is possible to calculate the resonance frequencies and the local vibration amplitudes and phases of the modes. Depending

* Corresponding author. Tel.: +49-681-93023935; fax: +49-681-93025903.

E-mail address: reinstaedtler@izfp.fhg.de (M. Reinstaedtler).

on the geometry of the beam analytical or numerical methods [20,21] can be used. However, the exact cantilever geometry is often not known and can vary considerably within one set of commercial beams. Properties of the beams, such as vertical and lateral spring constants are of fundamental importance for quantitative measurements, in particular for local elasticity measurements [20]. By examining the vibration spectra of the cantilevers during our ultrasonic AFM measurements, we often noticed the appearance of additional resonances not expected theoretically. Here we show that the free vibrational modes of clamped-free silicon AFM cantilevers can be imaged quantitatively. This provides evidence about the origin of the additional modes and also allows a quality control of AFM sensors because the effective spring constant depends on the vibrational mode of the cantilever [22], which in turn is influenced by the geometry of the cantilever, the mass distribution along its length, and the position of the tip.

2. Theory

2.1. Flexural vibrations

Bending and torsional vibrations of uniform, homogenous beams with constant rectangular cross-section can be described by a fourth- and a second-order partial differential equation, respectively. The equation of motion for the bending modes can be found in textbooks [23]

$$EI \frac{\partial^4 y}{\partial x^4} + \rho A \frac{\partial^2 y}{\partial t^2} = 0 \quad (1)$$

where E is the Young's modulus, $I = ab^3/12$ is the area moment of inertia of a beam with rectangular cross section, a is its width and b its thickness, ρ is the mass density and $A = ab$ is the cross sectional area. Here, x is the coordinate in the longitudinal direction of the cantilever, $y(x)$ is the excursion from the rest position of the length element at x . A general solution for Eq. (1) can be written as

$$y(x, t) = (a_1 e^{ix} + a_2 e^{-ix} + a_3 e^{i\gamma x} + a_4 e^{-i\gamma x}) e^{i\omega t} \quad (2)$$

Here, $\omega = 2\pi f$ is the angular frequency and $\gamma = 2\pi/\lambda$ the flexural wave number. Inserting Eq. (2) in Eq. (1) yields the dispersion relation

$$EI\gamma^4 - \rho A\omega^2 = 0 \quad (3)$$

or

$$\omega = \gamma^2 \sqrt{\frac{EI}{\rho A}} \quad (4)$$

The constants a_i ($i = 1, 2, 3, 4$) can be determined by the boundary conditions. In free vibrations, the cantilever is clamped at $x = 0$, whereas the free end is at $x = L$. This yields the characteristic equation for the wave number γ_n

$$\cos \gamma_n L \cosh \gamma_n L + 1 = 0 \quad (5)$$

Using Eq. (4) and the solutions $\gamma_n L$ of Eq. (5), one obtains the bending-mode eigenfrequencies

$$f_n = \frac{(\gamma_n L)^2}{2\pi L^2} \sqrt{\frac{b^2 E}{12\rho}} \quad (6)$$

The amplitude distribution of the flexural cantilever vibration $y_n(x)$ of each mode is described by the following equation

$$y_n(x) = y_0 \left[(\cos \gamma_n x - \cosh \gamma_n x) - \frac{\cos \gamma_n L + \cosh \gamma_n L}{\sin \gamma_n L + \sinh \gamma_n L} (\sin \gamma_n x + \sinh \gamma_n x) \right] \quad (7)$$

where y_0 is the vibrational amplitude.

2.2. Torsional vibrations

The equation of motion for torsional modes is

$$c_T \frac{\partial^2 \Theta}{\partial x^2} - \rho J \frac{\partial^2 \Theta}{\partial t^2} = 0 \quad (8)$$

where Θ is the angle of twist, $c_T = ab^3 G/3$ is the torsional stiffness and $J = a^3 b/12$ the polar area moment of inertia. A general solution for Eq. (7) can be written as

$$\Theta(x) = A \sin \eta x + B \cos \eta x \quad (9)$$

where constants A and B are also given by the clamped-free boundary conditions for the cantilever oscillations, so the amplitude distribution is

$$\Theta(x) = A \sin \eta x \quad (10)$$

The torsional wave number η is obtained by the balance of the torsional moments [12,24]

$$c_T \frac{\partial \Theta(x)}{\partial x} \Big|_{x=L} = 0$$

The eigenfrequencies for torsional vibrations are obtained by solving Eq. (8)

$$f_n = \frac{2n-1}{2} \underbrace{\frac{1}{L} \frac{b}{a} \sqrt{\frac{G}{\rho}}}_{\Delta f} \quad (11)$$

Unlike the bending mode eigenfrequencies (Eq. (6)) the torsional modes are equally spaced by Δf , because Eq. (8) exhibits no dispersion.

3. Experiments

3.1. Cantilever

The examined cantilevers were manufactured from highly doped, single-crystal silicon with integrated single-crystal silicon tip. The tip was pointing into the $\langle 100 \rangle$ direction, whereas the cantilever pointed into the $\langle 110 \rangle$ direction. We used two low force constant types designed for contact mode (Fig. 1) and for lateral force microscopy, respectively, from the same manufacturer (Pointprobe[®], Nanosensors, Wetzlar, Germany). For generating a high enough torsional vibration amplitude, we selected cantilevers with low bending and hence also low torsional stiffness. In order to determine the geometrical parameters, the width and length of the cantilevers were measured with an optical

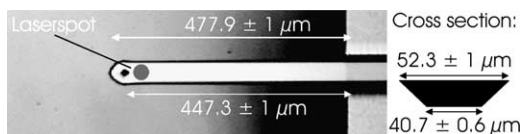


Fig. 1. Optical micrograph of the cantilever used for torsional mode measurement (type CONT); Calculated spring constant $k = 0.131$ N/m; nominal thickness: 2 ± 0.5 μm . The cantilever is supported by a single crystal silicon holder as can be seen on the right.

microscope. From the measured resonance frequency of the first ten bending modes the thickness of the cantilever was calculated using Eq. (6) avoiding time-consuming measurements using an electron-microscope.

3.2. Atomic force microscope set-up

The experimental set-up to measure the free vibration spectra of the cantilever with the AFM is shown in Fig. 2. A commercial Scanning Probe Microscope (Dimension 3000, Digital Instruments, Santa Barbara, CA) with additional ultrasonic equipment was used to excite and measure flexural and torsional vibration resonances of the cantilever. A frequency generator (HP 33120 A) provides a sinusoidal signal, which is applied to a conventional ultrasonic shear wave transducer (Panametrics V151, 5 MHz center frequency) attached to the sample. As a sample, we used a piece of a silicon wafer. The ensuing sample surface vibration couples via the air column between the cantilever and the sample into the cantilever mounted over the sample with a distance of about 2–5 μm . The cantilever vibrations were measured with the internal optical detector of the instrument, provided its bandwidth was in the MHz

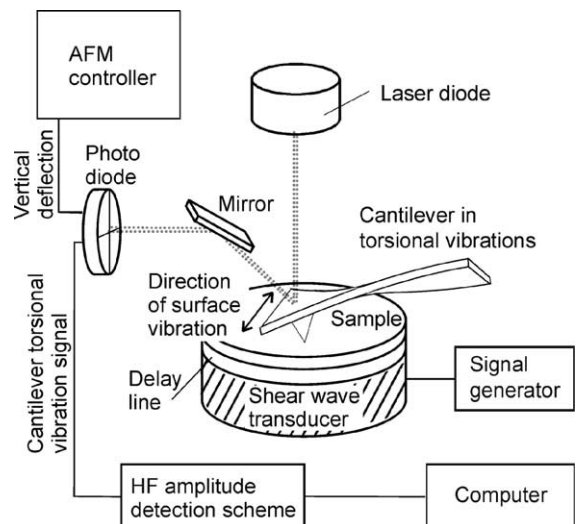


Fig. 2. Experimental set-up for torsional vibration measurements in an AFM.

regime, otherwise a fast external amplifying system was used. The HF amplitude detection scheme consists of a heterodyne down-converter which in addition receives a reference signal at the excitation frequency from the frequency generator. The heterodyne down-converter operates at frequencies from 75 kHz to 10 MHz and shifts the desired signal to a fixed 20 kHz intermediate frequency. It is evaluated by a lock-in amplifier. The set-up is controlled by a Labview program enabling one to change the frequency, to read the lock-in output, and to store the spectra.

Typical measured lateral vibration spectra of cantilever #1 (type CONT) are shown in Fig. 3. Besides torsional modes flexural modes also appeared in the lateral channel, however, never were torsional modes observed in the vertical channel. By calculating the first torsional eigenfrequency using Eq. (11), the 212 kHz peak in the lateral channel spectrum can be identified as belonging to a torsional resonance. However, a second peak appeared at 265.5 kHz without a corresponding peak in the vertical spectrum at the same frequency. In order to clarify the situation, we performed interferometric measurements of the displacements of the vibrating cantilevers in order to compare the experimentally determined vibration patterns to the expected patterns as calculated by Eqs. (7) and (11).

3.3. Interferometric measuring system

The interferometrical set-up is shown in Fig. 4. The chip of the cantilever was attached with a couplant to a shear ultrasonic transducer operated between 100 kHz and 3 MHz. It emitted into the

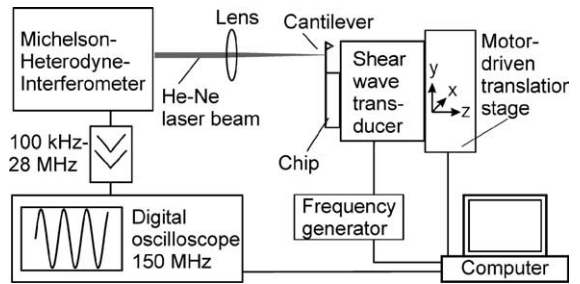


Fig. 4. Experimental set-up for imaging the resonance modes with an optical interferometer.

chip transverse waves polarized perpendicular to the long axis of the cantilever beam and parallel to its width causing forced vibrations. The absolute amplitudes of the cantilever vibrations were measured with an optical Michelson heterodyne interferometer [25]. The He-Ne laser beam of the interferometer was focused onto the cantilever with a spot diameter of 2–5 μm . Using a motor-driven linear translation stage, the focal spot of the interferometer was scanned over the surface of the cantilever. A step size of 2 μm was chosen. To determine the resonance frequencies, a spectrum was taken at a location close to the free end of the cantilever. Then the modes were imaged by scanning the vibrating cantilever at its resonance frequencies and detecting the deflection of each position as a function of time. The amplitude and phase of each time signal were obtained by using Digital Fourier Transformation.

The measured amplitude and phase distribution of the third bending mode of a 225 μm long beam are shown in Fig. 5. Two nodes and three crests of the vibration are found according to theory. The phase of the signal is measured relative to the

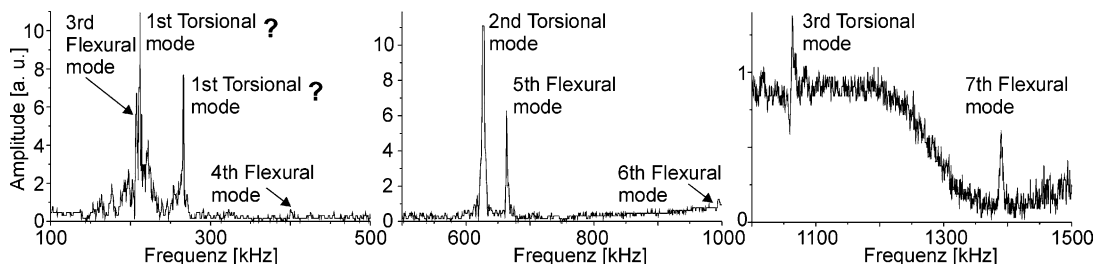


Fig. 3. AFM lateral channel spectra showing additional modes.

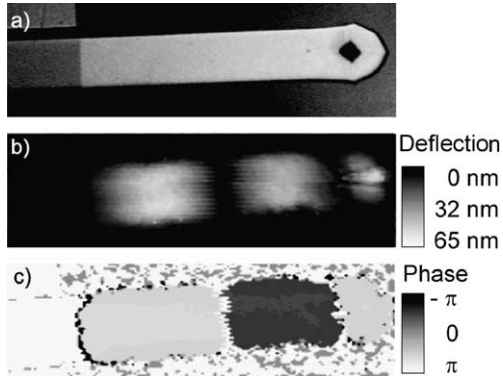


Fig. 5. (a) Optical micrograph of the cantilever measured; (b) amplitude and (c) phase distribution of the third bending mode of a rectangular cantilever. Scan size $300 \times 100 \mu\text{m}^2$.

excitation signal. The phase difference between two neighboring crests is π .

The first three torsional modes of the $450 \mu\text{m}$ long rectangular silicon-cantilever used for the AFM measurement described above are shown in Fig. 6. The amplitude and phase distribution of the second and third torsional mode agree very well to the theoretical prediction. It is interesting to note that the first two modes with eigenfrequencies close to one another do not correspond to the modes expected according to Eq. (11), as shown in Fig. 7. Additionally, the position of the center line deviates from the middle of the cantilever for all modes shown in Fig. 6. Note that the amplitudes of the bending modes were much higher than the amplitudes of the torsional modes, though the transducer mainly excited lateral oscillations of the

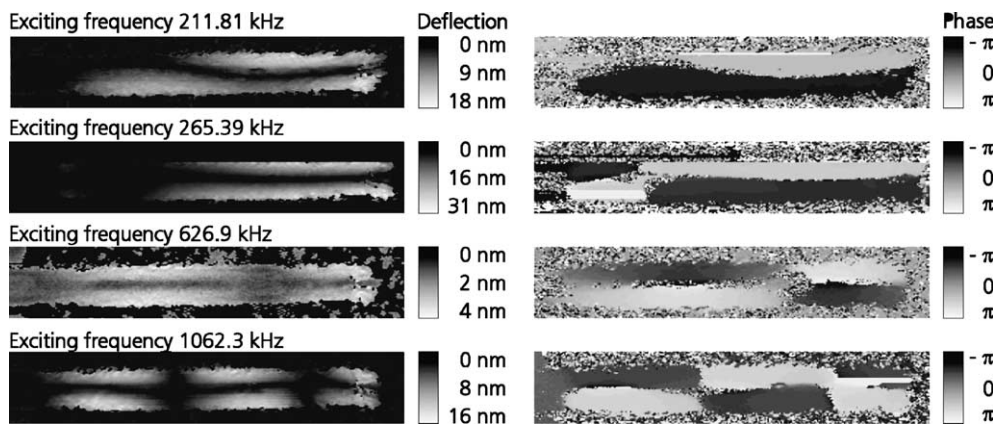


Fig. 6. Amplitude and phase distribution of the first three torsional modes of a rectangular Si-cantilever. The scan size is about $550 \times 100 \mu\text{m}^2$.

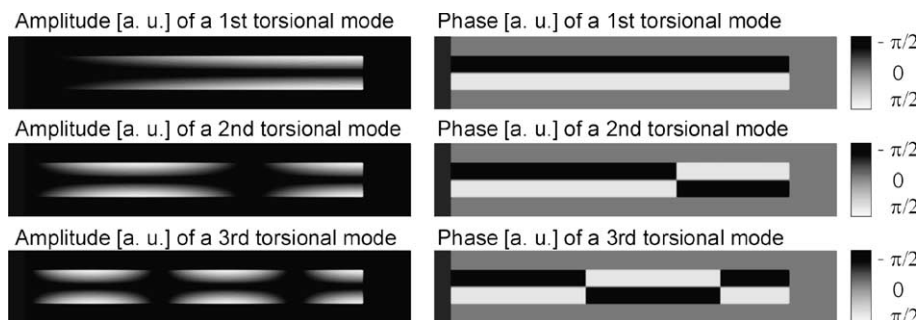


Fig. 7. Calculated amplitude and phase distribution of the first, second and third torsional mode.

cantilever base. This is caused by the lower bending stiffness of the cantilever compared to its torsional stiffness.

4. Mode coupling

We suggest that the origin of the asymmetrical shape of the modes is caused by geometrical asymmetries, mostly due to the tip positioned not exactly on the center line of the beam. These asymmetries in the vibration pattern entail a coupling of flexural and torsional vibrations via the tip when the tip is in force interaction with a sample surface. This holds in particular when additional static forces are applied in a measurement of elasticity [3]. Considering that the tip with the mass m_t is offset from the area center of the cross section by an amount d (see Fig. 8), the flexural and torsional modes are no longer independent. They couple via the forces acting on the tip and hence lead to an admixture of torsional motion in a flexural mode and vice versa. This coupling can be described by the Eqs. (1) and (8) taking account the following boundary conditions at the end with the tip ($x = L$)

$$EIy'''(x, t) = k_n y(x, t) - k_n \frac{d}{L} \theta(x, t) + m_t \left(\ddot{y}(x, t) - \frac{d}{L} \ddot{\theta}(x, t) \right) \quad (12)$$

$$c_T \theta'(x, t) = -k_t h^2 \theta(x, t) - k_n d L y(x, t) + m_t d (L \ddot{y}(x, t) - \ddot{\theta}(x, t)) \quad (13)$$

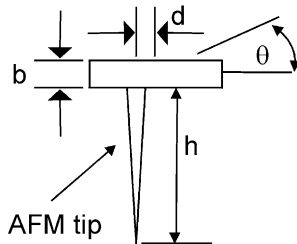


Fig. 8. Parameters entering in the description of mode coupling via the forces acting on an AFM tip of length h which is slightly offset by an amount d from the center-line of the beam.

k_l and k_n are the lateral and normal contact stiffness, respectively. Here, when the cantilever performs free oscillations, the boundary conditions reduce to

$$EIy'''(x, t) = m_t \left(\ddot{y}(x, t) - \frac{d}{L} \ddot{\theta}(x, t) \right) \quad (14)$$

$$c_T \theta'(x, t) = m_t d (L \ddot{y}(x, t) - \ddot{\theta}(x, t)) \quad (15)$$

This still leads to a coupling of the modes because the mass of the tip is not centered. Seeking harmonic solutions $y(x, t) = y(x)e^{i\omega t}$ and $\theta(x, t) = \theta(x)e^{i\omega t}$ leads to the characteristic equations

$$EIy'''(x) = m_t \omega^2 \left(\frac{d}{L} \theta(x) - y(x) \right) \quad (16)$$

$$c_T \theta'(x) = m_t d \omega^2 (d \theta(x) - L y(x)) \quad (17)$$

Inserting Eqs. (2) and (10) into Eqs. (16) and (17) leads to the relation $\eta = H\gamma^2$ between the flexural and torsional wave numbers γ and η where

$$H = \sqrt{EIJ/Ac_T L^2} \quad (18)$$

It is this parameter H which determines the likelihood of modal coupling. The mode shape of the peak at 212 kHz is a combination of the flexural and torsional solution. The weighting of the combined solutions depends on the type of and degree of coupling as well as on the excitation method. Two modes have frequencies very close to each other. The frequencies of the third flexural mode and the first torsional mode lie within 5% of each other. Thus, during forced vibrations, they are often excited simultaneously. Fig. 9 shows a plot of the combination of the first torsional and the third flexural mode.

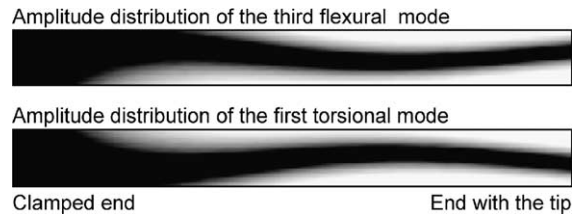


Fig. 9. Spatial plots of modes 3 and 4 calculated from the flexural/torsional coupling model with $H = 0.025$. When the frequencies are close together small perturbations cause these modes to couple.

A resonance was also observed at 265 kHz. The corresponding mode does not fit into an analysis based on mode coupling as explained above. Most likely, this mode originates from nonlinear coupling into flexural motion about an axis perpendicular to the plan view. Such a mode would have f_1 about $a/b = 22.5$ times the usual f_1 for flexure. This value matches with the observed frequency at 265 kHz. Calculating the elastic strain amplitudes prevailing in the beams for both modes, i.e. $\varepsilon_{\text{flex}} = (b/2)(d^2y/dx^2)$ and $\varepsilon_{\text{tors}} \approx \theta a/L$ (Eqs. (7) and (10)) and using the measurements for the amplitudes as shown in Figs. (5) and (6), one obtains values of the order $\varepsilon_{\text{flex}} \approx 10^{-5}$ and $\varepsilon_{\text{tors}} \approx 10^{-4}$. These rather large values make non-linear mixing of modes based on higher-order elasticity possible [26].

5. Conclusion

In summary, we have shown that mode coupling due to geometrical and mass asymmetries account for a number of resonances besides the standard flexural and torsional modes. The coupled modes can be observed in many commercial cantilevers. They are sometimes called spurious modes, yet they can be explained using quite simple physical principles. The large strains values obtained in dynamic operations may lead to non-linear mixing of modes.

Acknowledgements

This work was supported by the German Science Foundation through various grants. One of us (M.R.) is supported by a stipend via the Graduate College on “Advanced Materials for Efficient Energy Conversion”. The support of the U.S. Air Force Office of Scientific Research (grant no. F49620-99-1-0254) for J.A.T. is gratefully acknowledged. We also thank U. Hartmann, Department of Experimental Physics, University of the Saarland, for discussions.

References

- [1] G. Binnig, C.F. Quate, C. Gerber, *Phys. Rev. Lett.* 56 (1986) 930.
- [2] C.M. Mate, G.M. McClelland, R. Erlandsson, S. Chiang, *Phys. Rev. Lett.* 59 (1987) 1942.
- [3] U. Rabe, S. Amelio, M. Kopycinska, S. Hirsekorn, M. Kempf, M. Göken, W. Arnold, *Surf. Interface Anal.* 33 (2002) 65, and references contained therein.
- [4] O. Marti, J. Colchero, J. Mlynek, *Nanotechnology* 1 (1990) 141.
- [5] G. Meyer, N.M. Amer, *Appl. Phys. Lett.* 57 (1990) 2089.
- [6] P. Maivald, H.-J. Butt, S.A.C. Gould, C.B. Prater, B. Drake, J.A. Gurley, V.B. Elings, P.K. Hansma, *Nanotechnology* 2 (1991) 103.
- [7] T. Göddenhenrich, S. Müller, C. Heiden, *Rev. Sci. Instrum.* 65 (1994) 2870.
- [8] K. Yamanaka, E. Tomita, *Jpn. J. Appl. Phys.* 34 (1995) 2879.
- [9] J. Colchero, M. Luna, A.M. Baró, *Appl. Phys. Lett.* 68 (1996) 2896.
- [10] R.W. Carpick, D.F. Ogletree, F. Salmeron, *Appl. Phys. Lett.* 70 (1997) 1548.
- [11] J. Kerssemakers, J.Th.M. De Hosson, *Surf. Sci.* 417 (1998) 281.
- [12] K. Yamanaka, S. Nakano, *Appl. Phys. A* 66 (1998) 313.
- [13] K. Yamanaka, A. Noguchi, T. Tsuji, T. Koike, T. Goto, *Surf. Interface Anal.* 27 (1999) 600.
- [14] H.-U. Krottil, E. Weilandt, Th. Stifter, O. Marti, S. Hild, *Surf. Interface Anal.* 27 (1999) 341.
- [15] H.-U. Krottil, Th. Stifter, O. Marti, *Rev. Sci. Instrum.* 71 (2000) 2765.
- [16] H.-U. Krottil, Th. Stifter, O. Marti, *Rev. Sci. Instrum.* 72 (2001) 150.
- [17] P.-E. Mazeran, J.-L. Loubet, *Tribol. Lett.* 7 (1999) 199.
- [18] A. Szychalski-Merle, K. Krischker, T. Göddenhenrich, C. Heiden, *Appl. Phys. Lett.* 77 (2000) 501.
- [19] T.R. Albrecht, S. Akamine, T.E. Carver, C.F. Quate, *J. Vac. Sci. Technol. A* 8 (1990) 3386.
- [20] U. Rabe, K. Janser, W. Arnold, *Rev. Sci. Instrum.* 67 (1996) 3281.
- [21] T. Drobek, R.W. Stark, M. Gräber, W.M. Heckl, *New J. Phys.* 1 (1999) 15.1.
- [22] J.A. Turner, S. Hirsekorn, U. Rabe, W. Arnold, *J. Appl. Phys.* 82 (1997) 966.
- [23] L. Landau, E.M. Lifschitz, *Lehrbuch der theoretischen Physik, Auflage Bd. 7* (1991) 7.
- [24] K. Yamanaka, S. Nakano, *Appl. Phys. A* 66 (1998) 313.
- [25] B. Cretin, P.E. Mazeran, J.L. Loubet, *Tribol. Lett.* 3 (1995) 125.
- [26] A.H. Nayfeh, *Nonlinear Interactions*, John Wiley and Sons, New York, 2000, p. 542.